Fracture Mechanics of Concrete Structures, de Borst et al (eds) © 2001 Swets & Zeitlinger, Lisse, ISBN 90 2651 825 0

A Basic Creep Model for Concrete Subjected to Multiaxial Loads

F.Benboudjema, F.Meftah & A.Sellier
LGCU, Université de Marne-La-Vallée, France

G.Heinfling
EDF - DRD - MTC, Moret Sur Loing, France

J.M.Torrenti
Ecole Nationale des Ponts & Chaussées, France

ABSTRACT: A new model for basic creep of concrete under multiaxial compressive stresses is proposed. The basic creep is considered to be the result of two processes, which are driven by spherical and deviatoric components of the stress tensor, respectively. Each part of the creep deformation process is associated with a physical mechanism. The first one is the migration of the adsorbed water in the macro-porosity. The second mechanism corresponds to the sliding of C-S-H gel sheets. The basic creep model has been coupled with an isotropic damage model coupled with plasticity. Some numerical simulations are performed. They show that the model response fits pretty much with experiments, as far as multiaxial loads are concerned.

1 INTRODUCTION

Measurements in EDF's[1] pre-stressed concrete structures show a significant increase of the long-term strains with respect to the expected ones. The major suspected reason is that the initial design calculations are based on models which did not predict properly the occurrence of shrinkage and creep in concrete, when subjected to multiaxial loads, especially.

Indeed, most of the models for concrete creep have been developed in order to predict the longitudinal strains of concrete under uniaxial compressive loads. These models usually are extended to multiaxial loads by analogy to the classical Hooke's elasticity law by using a creep Poisson's ratio. Furthermore, most of the authors consider this creep Poisson's ratio as constant and equal to the elastic Poisson ratio (Bažant et al. 1997, Granger 1996). However, several experimental studies on basic creep of concrete under multiaxial compressive stresses show that the corresponding creep Poisson ratio is not constant with time. Its initial value is less than the elastic one (Gopalakrishnan et al. 1969, Jordaan et al. 1969). It rather depends upon the multiaxial character of the stress state and thus is non-isotropic. The former point (a constant Poisson ratio) implies that one can underestimate the basic creep strains of about 5 to 44 % (Benboudjema 1999). It may explain the increase of the long-term strains mentioned above, and the unexpected great deflection of some concrete bridges, which are longitudinally and transversally pre-stressed. The latter point implies that the superposition principle is no more valid. Moreover, a probabilistic calculus on a biaxial pre-stressed structure showed that the importance of the creep Poisson's ratio become predominant after about ten years for the estimation of long-term strains (Heinfling et al. 1998).

In this contribution, a new model for basic creep of concrete under multiaxial compressive stresses is proposed. The basic creep model has been implemented into a finite elements code. The creep model is coupled with an isotropic damage model coupled with plasticity in which the effective stress concept has been introduced. A mechanical damage variable is introduced to describe the degradation of the stiffness due to progressive microcracking. The damage variable is splitting up into two damage scalars depending on the sign of the stress in order to reproduce the crack closure effects when the material is subjected to alternated loads. This concrete model is also based on the non-associated flow theory of plasticity with a scalar hardening parameter, in order to describe correctly the dilatancy phenomenon. A multi-surfaces criterion is used so as to reproduce a suitable behavior of concrete in compression and in tension. The model is illustrated through some uniaxial and multiaxial creep tests existing in the literature.

2 MODELING OF BASIC CREEP OF CONCRETE

2.1 *Mechanisms and assumptions on basic creep of concrete*

In this model, the basic creep is considered to be the result of two processes, which are driven by the spherical and deviatoric components of the stress tensor, respectively. Several experimental findings prove that the splitting of the creep strain process to a spherical part and a deviatoric part is relevant (Glücklich et al. 1972, Gopalakrishnan et al. 1969, Jordaan et al. 1969). Moreover, they showed that the spherical creep strains and the deviatoric creep strains are proportional to the spherical part and the deviatoric part of the stress tensor, respectively.
Each part of the creep strain process is associated with a physical mechanism.
The spherical creep mechanism concerns water moving in both capillary space (reversible) and intrinsic porosity (irreversible), due to the hydrostatic component of the stress tensor. This is shown in figure 1.
The macroscopic spherical loading is firstly transmitted to the water adsorbed between the hydrated products, in the form of a pressure. The water involved will therefore migrate reversibly to the non-saturated capillary space (see 1 in Figure 1), without any increase of the capillary pore pressure.

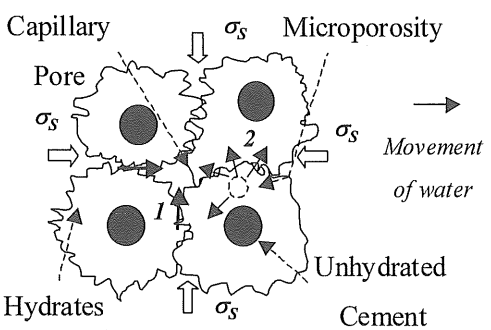

Figure 1. Proposed mechanism for the spherical creep. (Benboudjema 1999)

When the skeleton is progressively loaded, the macroscopic spherical loading is then retransmitted to the water adsorbed in the intrinsic porosity of the hydrates, which will migrate (see 2 in Figure 1) to the capillary pore too, but this movement is now irreversible due to capillary tensions. Several tests confirmed the partially reversible character of the spherical creep strain (Glücklich et al. 1972, Gopalakrishnan et al. 1969, Jordaan et al. 1969).

The first mechanism is similar to the one proposed by Ulm et al. (1998), and has been related to the short-term creep. As for the second mechanism, the water migration is much slower due to the high complexity of the microstructure of the hydrated products, and is therefore related to the long-term creep.
It is here assumed that the spherical creep strain of concrete is asymptotic because the water is available only in a finite quantity. This assumption has been verified experimentally (Glücklich et al. 1972). The volumetric basic creep of the mortars subjected to a hydrostatic compression ceased after about 40 days.
The deviatoric creep mechanism is presented in Figure 2.
The macroscopic deviatoric loading is transmitted at the microporosity scale, which will drive the sliding of the C-S-H sheets. As in the case of the spherical mechanism, we split up the deviatoric creep strain in a reversible and an irreversible component (confirmed by several tests, see Benboudjema et al. 2000). The water absorbed (see 1 in Figure 2) near the C-S-H gel wall (with a great absorption energy) is responsible for the reversible aspect of the deviatoric creep; after unloading, it will drive back the C-S-H sheet sliding, due to its load-bearing character. After some water layers (see 2 in Figure 2), the absorption energy is much lower, therefore the movement of this water is not reversible.

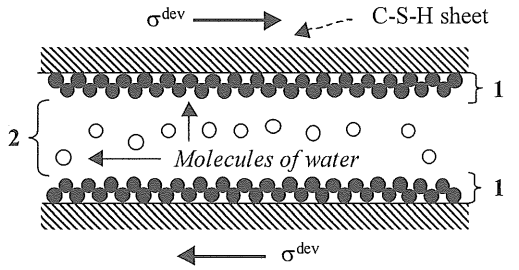

Figure 2. Mechanisms of the deviatoric creep in the C-S-H micropores. (Benboudjema 1999)

We will present now the constitutive equations of the model.

2.2 *Constitutive relations of the basic creep model*

The spherical and deviatoric part of the creep strain tensor ($\boldsymbol{\varepsilon}^{sph}$ and $\boldsymbol{\varepsilon}^{dev}$ respectively) are derived from the creep strain tensor $\boldsymbol{\varepsilon}$ by the following manner:

$$\boldsymbol{\varepsilon}^{sph} = p \cdot 1 \text{ with } p = \frac{1}{3} \cdot tr(\boldsymbol{\varepsilon}) = \frac{1}{3} \cdot (\varepsilon_{11} + \varepsilon_{22} + \varepsilon_{33}) \quad (1)$$

$$\boldsymbol{\varepsilon}^{dev} = \boldsymbol{\varepsilon} - \boldsymbol{\varepsilon}^{sph} \tag{2}$$

where ε_{11}, ε_{22} and ε_{11} are the principal creep strain. The corresponding spherical and deviatoric stress ($\boldsymbol{\sigma}^{sph}$ and $\boldsymbol{\sigma}^{dev}$ respectively) are obtained by the same manner.

The creep Poisson's ratio is calculated by the following equation (where J is the creep compliance) for a system of multiaxial stresses:

$$\varepsilon_{ii} = J \cdot \left(\sigma_i - \nu_i \cdot \left[\sigma_j + \sigma_k\right]\right) \Rightarrow \nu_i = \left(\frac{\sigma_i - \dfrac{\varepsilon_{ii}}{J}}{\sigma_j + \sigma_k} \right) \tag{3}$$

The creep compliance can be obtained by a uniaxial creep companion test:

$$\varepsilon_u = J \cdot \sigma_u \Rightarrow J = \frac{\varepsilon_u}{\sigma_u} \tag{4}$$

where ε_u is the longitudinal creep strain, and σ_u the applied stress.

The physical mechanism of the spherical creep leads to a model presented in details by Benboudjema (1999). The spherical creep strain can be therefore expressed by the following expressions:

$$\begin{cases} \dot{\varepsilon}^{sph} = \dfrac{1}{\eta_r^{sph}} \cdot \left[\sigma^{sph} - k_r^{sph} \cdot \varepsilon_r^{sph}\right] - \dot{\varepsilon}_i^{sph} \\ \dot{\varepsilon}_i^{sph} = \dfrac{1}{\eta_i^{sph}} \left\langle \left[k_r^{sph} \cdot \varepsilon^{sph} - \left(k_r^{sph} + k_i^{sph}\right) \cdot \varepsilon_i^{sph}\right] \right. \\ \qquad \left. - \left[\sigma^{sph} - k_r^{sph} \cdot \varepsilon_r^{sph}\right] \right\rangle^+ \end{cases} \tag{5}$$

$$\varepsilon^{sph} = \varepsilon_r^{sph} + \varepsilon_i^{sph} \text{ with } \langle x \rangle^+ = \frac{x + |x|}{2} \tag{6}$$

where ε_r^{sph} and ε_i^{sph} are the reversible and the irreversible spherical creep strain respectively ; η_r^{sph} and η_i^{sph} are the apparent viscosities of the water at two different scales of the material (macroscopic and microscopic level, respectively). These apparent quantities depend upon the water viscosity and the connected porosity geometry. Further, k_r^{sph} and k_i^{sph} are the apparent stiffness associated to the precedent viscosities and related to the stiffness of the porous material and the skeleton.

The differential equations system (5) is coupled and can not be solved directly if $d\varepsilon_i^{sph} \neq 0$. This system can be written on a matrix form:

$$\dot{\boldsymbol{\varepsilon}}^{sph} = \mathbf{A} \cdot \boldsymbol{\varepsilon}^{sph} + \sigma^{sph} \cdot \mathbf{B} \tag{7}$$

where $\boldsymbol{\varepsilon}^{sph}$ is the vector of the reversible and irreversible basic creep strains.

Let us decompose the matrix, **A**, in its eigenvector base:

$$\mathbf{A} = \mathbf{P} \cdot \mathbf{D} \cdot \mathbf{P}^{-1} \tag{8}$$

where **P** is the matrix of the eigenvectors and **D** is a diagonal matrix.

The spherical creep strains can be expressed in the eigenvector base. The differential equations system (5) can now be expressed in an uncoupled form:

$$\dot{\boldsymbol{\varepsilon}}_*^{sph} = \mathbf{D} \cdot \boldsymbol{\varepsilon}_*^{sph} + \sigma^{sph} \cdot \mathbf{P}^{-1} \cdot \mathbf{B} \tag{9}$$

where $\boldsymbol{\varepsilon}_*^{sph}$ is the spherical creep vector expressed in the eigenvector base.

Therefore, the expression of the spherical creep strain vector can be derived from the equation (9) in the eigenvector base and then in the original base after a base transformation. The expressions of the reversible and irreversible creep strains are:

$$\begin{cases} \varepsilon_r(t) = \dfrac{\sigma^{sph}}{k_r^{sph}} + \sigma^{sph} \cdot \left(a_{11} \cdot \exp\left(-\dfrac{t}{\tau_1}\right) + a_{12} \cdot \exp\left(-\dfrac{t}{\tau_2}\right) \right) \\ \varepsilon_i(t) = \dfrac{\sigma^{sph}}{k_i^{sph}} + \sigma^{sph} \cdot \left(a_{21} \cdot \exp\left(-\dfrac{t}{\tau_1}\right) + a_{22} \cdot \exp\left(-\dfrac{t}{\tau_2}\right) \right) \end{cases} \tag{10}$$

where a_{11}, a_{12}, a_{21}, a_{22}, τ_1 and τ_2 are parameters which depend on η_r^{sph} ,η_i^{sph}, k_r^{sph} and k_i^{sph} (Benboudjema 2001).

The physical mechanism of the deviatoric creep leads also to a model presented in details in (Benboudjema 1999). The constitutive equations of the model are:

$$\begin{cases} \varepsilon_{ii}^{dev} = \varepsilon_{ii}^{dev}(rev) + \varepsilon_{ii}^{dev}(ire) \\ \eta_r^{dev} \cdot \dot{\varepsilon}_{ii}^{dev}(rev) + k_r^{dev} \cdot \varepsilon_{ii}^{dev}(rev) = \sigma_{ii}^{dev} \\ \eta_i^{dev} \cdot \dot{\varepsilon}_{ii}^{dev}(ire) = \sigma_{ii}^{dev} \end{cases} \tag{10}$$

The deviatoric creep strain can be therefore expressed analytically by the following equation:

$$\varepsilon_{ii}^{dev}(t) = \left[\frac{1}{\eta_i^{dev}} \cdot t + \frac{1}{k_r^{dev}} \cdot \left(1 - \exp\left(-\frac{k_r^{dev}}{\eta_r^{dev}} \cdot t\right)\right) \right] \cdot \sigma_{ii}^{dev} \tag{11}$$

The total creep strains are the sum of the spherical creep strain and the deviatoric creep strains:

$$\varepsilon_{ii} = \varepsilon^{sph} + \varepsilon_{ii}^{dev} = J_{sph} \cdot \sigma^{sph} + J_{dev} \cdot \sigma_{ii}^{dev} \tag{12}$$

Some numerical simulations will now be performed.

2.3 *Validation of the basic creep model*

For the validation of the model, we use the experimental results from Gopalakrishnan et al. (1969). The concrete specimens were 10 in. (25.4 cm) cubes and were cured and stored at 98 ± 2 % H.R. The water-cement ratio was 0.72. The specimen was

loaded at an age of 8 days (with a nominal strength of 29 MPa, at this time), then unloaded at an age of 36 days. At first, the parameters of the model are identified on the spherical and deviatoric part of the creep strain tensor for a biaxial test. The applied stresses are given in Table 1:

Table 1. Applied stresses at 8 days during the biaxial test.

σ_1 [MPa]	σ_2 [MPa]	σ_3 [MPa]
12.54	7.25	0

And the values of the parameters are given in Table 2:

Table 2. Values of the identified parameters.

Spherical Part

k_r^{sph} [MPa]	k_i^{sph} [MPa]	η_r^{sph} [MPa.s]	η_i^{sph} [MPa.s]
$2.46\ 10^5$	$7.09\ 10^4$	$3.3\ 10^9$	$6.49\ 10^{10}$

Deviatoric Part

k_r^{dev} [MPa]	η_r^{dev} [MPa.s]	η_i^{dev} [MPa.s]
$4.96\ 10^4$	$2.54\ 10^{10}$	$3.91\ 10^{11}$

To obtain the optimum values of the model parameters, a nonlinear optimization program (based on the Levenberg-Marquardt algorithm) is used (Benboudjema 2001) by minimizing the sum of the squares of the deviations from the data points.

The result of the identification is given in Figure 3, for the total creep strain (ε_{11}, ε_{22} and ε_{33}), after considering each mechanism alone:

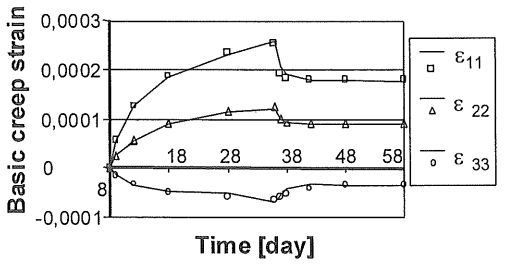

Figure 3. Simulation of the basic creep strains (2D test).

Next, we used the parameters determined above to simulate the longitudinal creep strain of a uniaxial companion test (σ = *12,5 MPa*), performed on the same concrete mixture. The result of the simulation is given in Figure 4 (ε_u). The attempt is to show how the model is able to reproduce the results of the associated uniaxial test with a parameter set identified from a biaxial test.

The calibration and the simulation give good agreements with the test results. The model does not underestimate the creep strains in the uniaxial and the biaxial test. The Figure 4 shows the evolution of

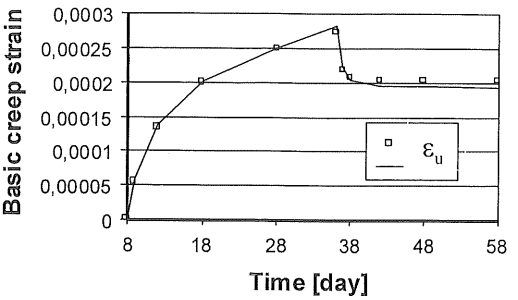

Figure 4. Simulation of the longitudinal basic creep strains (1D test).

creep Poisson's ratio with time and direction. It is calculated from the expressions given by the equation (3) and (4).

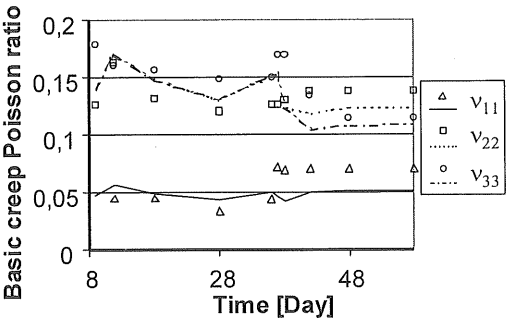

Figure 5. Evolution of the basic creep Poisson's ratio.

The model can predict a creep Poisson's ratio very close to the experimental one. It depends on the direction and on time. It is four times smaller than the elastic Poisson's ratio in the most loaded direction. Therefore taking a creep Poisson ratio equal to the elastic one underestimate the creep strain in that direction (see equation (3)).

Note that the inverse procedure in which the simulation of multiaxial creep tests with a parameter set identified from a uniaxial test does give similar results (Benboudjema 1999).

3 IMPLEMENTATION OF THE BASIC CREEP MODEL COUPLED WITH A MECHANICAL MODEL INTO A FINITE ELEMENTS CODE

3.1 *Constitutive relations of the mechanical model*

The basic creep model has been implemented into a finite elements code. The creep model is coupled with an isotropic damage model coupled with plasticity (Nechnech 2000). The damage variable is associated to the mechanical degradation process of concrete induced by the development of mi-

crocracks. It is defined as the ratio between the area occupied by created micro-cracks, over the whole material area (see figure 6).

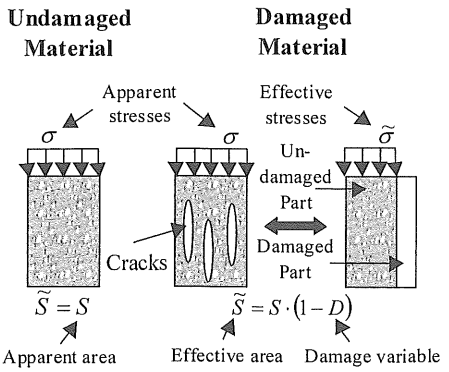

Figure 6. Definition of the damage variable.

Since the behavior of the undamaged part of the material is elastic, the stress-strain relationship reads:

$$\boldsymbol{\sigma} = (1 - D) \cdot \tilde{\boldsymbol{\sigma}} = \mathbb{E}_0 \cdot (1 - D) \cdot \boldsymbol{\varepsilon}_e \tag{13}$$

where $\mathbb{E}_0$ is the initial elastic stiffness matrix, $\boldsymbol{\varepsilon}_e$ is the elastic strains vector and D is the isotropic scalar damage variable.

The damage variable represents the effect of progressive microcracking, due to external mechanical loads, in term of degradation of the current Young's modulus of the material. The evolution of the damage variable is an exponential form:

$$D_x = 1 - \exp(c_x \cdot f(t) \cdot \kappa_x) \tag{14}$$

where κ_x is the cumulative plastic strain driving in fact the cracking process, c_x a material parameter and $f(t)$ a function which depends on current time. The subscript x refers to traction (t) or compression (c).

The signification of the f function comes from the manifestation of time-dependent growth of microcracks, initiated by gradual breakage of bonds. This function reads:

$$\begin{cases} f(t) = \exp\left[-\left(\dfrac{t}{\tau} \right)^{\mu} \right] & \text{if } \kappa_x \neq 0 \\ \dot{f}(t) = 0 \text{ if } \kappa_x = 0 \end{cases} \tag{15}$$

where τ and μ are constant parameters.

In order to describe properly the differences in the behavior of concrete in compression and in tension, the damage variable is separated into a compressive one and tension one. The crack closure effect is taken into account by multiplying the damage variable in tension with a scalar weight factor p. This scalar reflects the elastic stiffness recovery during the unloading process from tension state to compression state:

$$1 - D = (1 - D_c) \cdot (1 - p \cdot D_t)$$

$$p = \frac{\sum_{i=1}^{i=3} \left\langle \tilde{\sigma}_i \right\rangle}{\sum_{i=1}^{i=3} \left| \tilde{\sigma}_i \right|} \quad with \left\langle \tilde{\sigma}_i \right\rangle = \left(\tilde{\sigma}_i + \left| \tilde{\sigma}_i \right| \right) / 2 \tag{16}$$

Here, we consider the partition of the total strain. The strain increment is decomposed into an elastic one, a plastic and a creep one:

$$\dot{\boldsymbol{\varepsilon}} = \dot{\boldsymbol{\varepsilon}}_e + \dot{\boldsymbol{\varepsilon}}_p + \dot{\boldsymbol{\varepsilon}}_c \tag{17}$$

where $\boldsymbol{\varepsilon}_p$ and $\boldsymbol{\varepsilon}_c$ are the plastic and the creep strains vectors, respectively. The dot represents derivation respect to time.

The coupling between damage and plasticity is based on the definition of the effective stress in the material and on the assumption that the undamaged material is elasto-plastic (Ju 1989). In order to reproduce suitable behavior in compression and in tension (Feenstra 1993), a Drucker-Prager criterion in compression and a Rankine criterion in tension are used (see Figure 7).

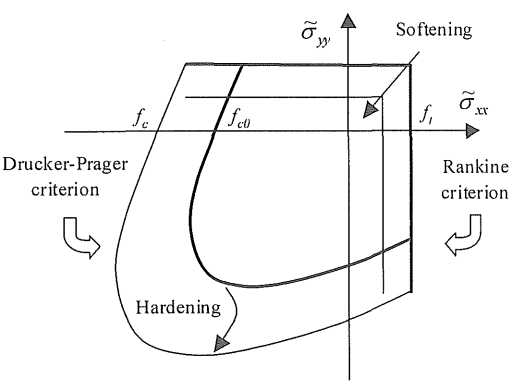

Figure 7. Drucker-Prager and Rankine criterion in the principal stress space (2D).

The Drucker-Prager criterion is written as:

$$F_c(\tilde{\boldsymbol{\sigma}}, \kappa_c) = J_2(\tilde{\mathbf{s}}) + \alpha_f \cdot I_1(\tilde{\boldsymbol{\sigma}}) - \beta \cdot \tilde{\tau}_c(\kappa_c) \tag{18}$$

where $J_2(\mathbf{s})$ is the second invariant of the deviatoric stress tensor $\mathbf{s}$, $I_1(\boldsymbol{\sigma})$ is the first invariant of the stress tensor $\boldsymbol{\sigma}$, τ_c is the nominal strength in compression, α_f and β are two material parameters.

The Rankine criterion is written as:

$$F_t(\tilde{\boldsymbol{\sigma}}, \kappa_t) = \tilde{\sigma}_I - \tilde{\tau}_t(\kappa_t) \tag{19}$$

where σ_I is the maximal principal stress in tension and τ_t is the nominal strength in tension.

The nominal strengths are defined by:

$$\tau_x = f_{x0}\left[\left(1+a_x\right)\exp\left(-b_x\cdot\kappa_x\right) - a_x\exp\left(-2b_x\cdot\kappa_x\right)\right]\cdot f(t) \tag{20}$$

where a_x and b_x are material parameters identified from uniaxial test (Nechnech 2000).
Note that the nominal strengths depend upon time, which means that the carrying capacity of the material decreases with time to take into account delay effect of cracks growth on strength evolution due to creep strains.
The non-associative plastic flow theory is adopted in compression in order to predict the correct amount of dilatation of concrete since the damage model is isotropic, which means the use of plastic potential that reads:

$$G_c = J_2(\tilde{\mathbf{s}}) + \alpha_g\, I_1(\tilde{\boldsymbol{\sigma}}) - \beta\,\tilde{\tau}_c(\kappa_c) \tag{21}$$

where α_g is a material parameter which controls dilatancy of concrete.
The plastic strain rate is then obtained by Koiter assumption:

$$\dot{\boldsymbol{\varepsilon}}^p = \dot{\lambda}_t \frac{\partial F_t}{\partial \tilde{\boldsymbol{\sigma}}} + \dot{\lambda}_c \frac{\partial G_c}{\partial \tilde{\boldsymbol{\sigma}}} \tag{22}$$

It is well established today that strain softening induces inherent mesh dependency and produces failure without energy dissipation (Bažant 1976). In order to avoid these unpleasant features, we use the fracture energy approach proposed by Hillerborg et al. (1976), which consists to introduce a characteristic length related to the size of the localized zone (Nechnech 2000).

3.2 *Coupling between the basic creep model and the mechanical model*

We suppose that basic creep only occurs in the undamaged part of the material. Therefore, the equation (12) reads:

$$\varepsilon_{c\,ii} = J_{sph}\cdot\tilde{\sigma}^{sph} + J_{dev}\cdot\tilde{\sigma}_{ii}^{dev} \tag{23}$$

The equation (23) assumes that nonlinear creep does not exist (Bažant et al. 1997). The nonlinearity observed in experimental tests comes from the growth of microcracks in time, which is taken into account by the equation (14) and (20).
In order to take into account the stress history, it is therefore possible to make use of the Boltzman superposition principle:

$$\varepsilon_{ii}(t) = \int_0^t \left(J_{sph}\cdot\dot{\tilde{\sigma}}^{sph} + J_{dev}\cdot\dot{\tilde{\sigma}}_{ii}^{dev}\right)d\tau \tag{24}$$

A major inconvenience of the previous equation is that one has to save the whole history of stresses in each Gauss points in the case of a finite elements calculus. If the number of finite elements or/and the number of time steps are numerous, the saved data quantity may be so important and makes the numerical calculus impossible to be achieved with reasonably memory loads.
This major disadvantage can be avoided in the present model. During a time-step, the stress history is approximated by a linear function (Bažant et al. 1982):

$$\tilde{\boldsymbol{\sigma}}(t) = \tilde{\boldsymbol{\sigma}}_n + \Delta\tilde{\boldsymbol{\sigma}}_n \frac{(t-t_n)}{\Delta t_n} \; with \begin{cases} t\in[t_n, t_{n+1}] \\ \Delta t_n = t_{n+1} - t_n \\ \Delta\tilde{\boldsymbol{\sigma}}_n = \tilde{\boldsymbol{\sigma}}_{n+1} - \tilde{\boldsymbol{\sigma}}_n \end{cases} \tag{25}$$

where $\boldsymbol{\sigma}_n$ is the stress vector at time step number n, and t_n is the time at time-step number n.
By solving the differential equation (5) and (10) with the approximation of stresses (25), the basic creep strains reads now (Benboudjema et al. 2001):

$$\boldsymbol{\varepsilon}_c^{n+1} = \mathbf{A}\cdot\tilde{\boldsymbol{\sigma}}_n + \mathbf{B}\cdot\tilde{\boldsymbol{\sigma}}_{n+1} + \mathbf{C}\cdot\boldsymbol{\varepsilon}_c^n \tag{26}$$

where $\boldsymbol{\varepsilon}_c{}^n$ is the basic creep strains vector at time-step number n, $\mathbf{A}$, $\mathbf{B}$ and $\mathbf{C}$ are squared matrix which depends only upon material parameters, t_n and Δt.
Therefore, we just need to save the stresses vector and the creep strains vector at time step number n to know the basic creep strains vector at time-step number $n+1$. The stress vector at the end of the time step number $n+1$ is written as:

$$\tilde{\boldsymbol{\sigma}}_{n+1} = \mathbf{E}_0\cdot\boldsymbol{\varepsilon}_e^{n+1} = \mathbf{E}_0\cdot\left(\boldsymbol{\varepsilon}^{n+1} - \boldsymbol{\varepsilon}_p^{n+1} - \boldsymbol{\varepsilon}_c^{n+1}\right) \tag{27}$$

where $\boldsymbol{\varepsilon}_e{}^n$, $\boldsymbol{\varepsilon}^n$ and $\boldsymbol{\varepsilon}_p{}^n$ are the elastic, total and plastic strains vector at time step number n, respectively.
Finally, if one makes use of the equation (26), the stress vector at the end of the time step reads:

$$\begin{cases} \tilde{\boldsymbol{\sigma}}_{n+1} = \mathbf{H}_{n+1}^{-1}\cdot\left(\tilde{\boldsymbol{\sigma}}_{n+1}^{tr} - \mathbf{E}_0\cdot\boldsymbol{\varepsilon}_p^{n+1}\right) \\ \mathbf{H}_{n+1} = \left(\mathbf{I}+\mathbf{B}\right) \\ \tilde{\boldsymbol{\sigma}}_{n+1}^{tr} = \mathbf{E}_0\cdot\left(\boldsymbol{\varepsilon}^{n+1} - \boldsymbol{\varepsilon}_p^n - \mathbf{A}\cdot\tilde{\boldsymbol{\sigma}}_n - \mathbf{C}\cdot\boldsymbol{\varepsilon}_c^{n+1}\right) \end{cases} \tag{28}$$

where $\mathbf{I}$ is the unit matrix and $\boldsymbol{\sigma}_{n+1}{}^{tr}$ is the trial stress vector, which can be calculated at the beginning of the time step, since all the involved quantities are known.
The effect of creep can therefore be taken into account easily, without any noticeable change in the existing resolution algorithm of the plastic model (Nechnech 2000).
Some numerical simulations will now be performed.

3.3 *Validation of the mechanical model*

For the validation of the model, we use the experimental results from Li (1994). The concrete prismatic specimens were 10 × 10 × 50 cm and were sealed by wax. The storage and test temperature was 20 ± 1°C. The water-cement ratio was 0.67. The Young modulus of the specimens was 25.8 GPa, the

elastic Poisson ratio, 0.14 and the ultimate strength in compression, 9.8 – 12.75 MPa. Specimens were loaded in uniaxial compression until the failure occurred. The stress levels were 83, 85, 90 and 95 percent of ultimate strength.
Since we do not have the experimental stress-strain curve for the tested specimens, we use typical parameters in order to describe the behavior of concrete in compression. The values of the mechanical parameters are identified from conventional uniaxial compressive tests and are listed in Table 3.

Table 3. Values of the mechanical parameters used in the simulations.

a_c	b_c	c_c	α_f	β	α_g
11.24	435	142	0.1212	0.8787	0.2

In the case of uniaxial loading, it is possible to link the time when failure occurs to the ratio of the applied stress over the ultimate strength. We obtain analytically by the combination of the equation (15) and (20):

$$t_f = -\tau \cdot \left(\ln\left(\frac{4 \cdot a_c}{(1+a_c)^2} \cdot \frac{\sigma_u}{f_{c0}} \right) \right)^{1/\mu} \qquad (29)$$

where t_f is the time at failure and σ_u the applied uniaxial stress.

Since we have experimental results on time at failure for different stress to strength ratio, we can identify the parameters τ and μ (Figure 8).

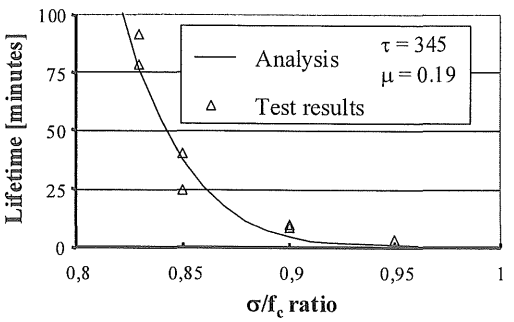

Figure 8. Time at failure versus stress to strength ratio.

The calibration of the parameters gives good agreement with the data for the lifetime of specimens. Note that if the applied uniaxial stress is equal to the ultimate strength, the specimen fails immediately, which is consistent with what we can except.
The creep parameters are identified from the axial and lateral creep measured strains in an uniaxial test. They are listed in Table 4:

Table 4. Values of the identified creep parameters.
Spherical Part

k_r^{sph} [MPa]	k_i^{sph} [MPa]	η_r^{sph} [MPa.s]	η_i^{sph} [MPa.s]
$2.09\ 10^5$	$7.44\ 10^4$	$1.99\ 10^5$	$8.85\ 10^{10}$

Deviatoric Part

k_r^{dev} [MPa]	η_r^{dev} [MPa.s]	η_i^{dev} [MPa.s]
$8.28\ 10^4$	$1.8\ 10^{10}$	$5.17\ 10^{11}$

The result of the simulation, for stress to strength ratio equal to 0.83, is given in Figure 9:

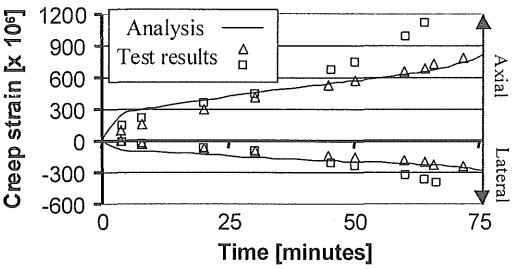

Figure 9. Creep strains in the axial and lateral directions versus time under sustained stress at 83 percent of ultimate strength.

From figure 9, we observe that the numerical results correlates quite well with the experimental data for the axial and the lateral creep strains.

4 CONCLUSION

To the authors knowledge, it is the first creep model for concrete which takes into account directly multiaxial loads, without using a creep Poisson's ratio, since its value depends here on the strain tensor buildup.
The preliminary results presented in this paper show that the model response fits pretty much with experiments, as far as multiaxial loads are concerned. The splitting of the creep strain in a spherical and a deviatoric component, as well as theirs mechanisms and descriptions seem to be relevant. However, precise experimental data are still needed in order to validate fully the hypotheses introduced in the proposed model and to allow its extension to take drying effects into account. In that aim, an important experimental research program including uniaxial as well as multiaxial creep tests is currently undertaken at EDF Research Division.
The basic creep model has also been coupled with an isotropic damage model coupled with plasticity. Creep is supposed to be proportional to effective stresses in the undamaged material. Growth of microcracks in concrete is taken into account in the

model, since the scalar damage variable and the nominal strengths depend both on time and the cumulative plastic strain. From the finite elements implementation point of view, the effect of creep is easily taken into account, since existing algorithms of the plastic model remains nearly unchanged. Numerical simulation shows that the model predicts correctly the lifetime of the specimen under uniaxial compression stresses for various stress to ultimate strength ratios. Moreover, the model response fits pretty much with both uniaxial and lateral experimental time-dependent strains.

REFERENCES

Bažant, Z.P. 1976. Instability, ductility and size effect in strain softening concrete. *journal of Engineering Mechanics ASCE* 102: 331-344.

Bažant, Z. P. & Wittman, F.H. 1982. *Mathematical modeling of creep and shrinkage of concrete.* John Wiley & Sons Limited: New York.

Bažant, Z.P. & Xiang, Y. 1997. Crack growth and life time of concrete under long time loading. *Journal of Engineering Mechanics* 123(4): 350-358.

Bažant, Z.P. & Hauggaard, A.B. & Baweja, S. & Ulm, F.J. 1997. Microprestress-Solidification Theory for Concrete Creep 1 : Aging and Drying Effects. *Journal of Engineering Mechanics* 123(11): 1188-1194.

Benboudjema, F. 1999. Modélisation des déformations différées du béton sous sollicitions biaxiales. Application aux bâtiment réacteurs de centrales nucléaires. *Rapport de D.E.A. de l'ENS Cachan*: 36. (*in french*)

Benboudjema, F. & Meftah, F. & Heinfling, G. 2000. Analyse des essais de fluage propre réalisés sur des pâtes de ciment, mortiers et bétons, avec mesures des déformations principales . *Rapport interne EDF:* 88. (in french)

Benboudjema, F. & Meftah, F. & Heinfling, G. 2001. Étude numérique et analytique de la partie sphérique du modèle de fluage propre LGCU. *Rapport interne EDF:* 55. (in french)

Feenstra, P.H. 1993. Computational aspects of biaxial stress in plain and reinforced concrete, *PhD thesis, Delft institute of technology*. Netherlands: 149.

Glucklich, J. & Amar, A. 1972. The Volumetric Creep of Mortars Subjected to Triaxial Compression, In *La déformation et la rupture des solides soumis à sollicitations pluriaxiales. Colloque international de la RILEM, Cannes, 4-6 octobre:* 79-95. Paris: Eyrolles.

Gopalakrishnan, K. S. & Neville, A.M. & Ghali A. 1969. Creep Poisson's Ratio of Concrete Under Multiaxial Compression. *ACI Journal* 66(90): p. 1008-1020.

Granger, L. 1996. Comportement Différé du Béton dans les Enceintes de Centrales Nucléaires : Analyse et Modélisation. *Thèse de doctorat de l'ENPC*: 398. Paris: LCPC. (*in french*)

Heinfling, G. & Courtois, A. & Hornet, P. 1998. Application des méthodes probabilistes à l'analyse du comportement des structures en béton armé vieillissantes : une approche industrielle. In *Fiabilité des structures, 2ème conférence nationale JN-FIAB'98, Marne-La-Vallée, 23-24 Novembre*: 231-246. Paris, Hermes. (*in french*)

Hillerborg, A. & Modeer, M. & Petersson, P.E. 1976. Analysis of crack formation and crack growth in concrete by means of fracture mechanics and finite elements. *Cement and Concrete Research* 6(6): 773-782.

Jordaan, I.J. & Illston, J.M. 1969. The Creep of Sealed Concrete under Multiaxial Compressive Stresses. *Magazine of Concrete Research* 21(69): 195-204.

Ju, J.W. 1989 On Energy-Based Coupled Elastoplastic Damage Theories: Constitutive Modeling and Computational Aspects. *International Journal of Solids and Structures* 25(7): 803-833.

Li, Z. 1994. Effective creep Poisson's ration for damaged concrete. *International Journal of Fracture* 66:189-196.

Nechnech, W. 2000. Contribution à l'étude numérique du comportement du béton et des structures en béton armé soumises à des sollicitations thermiques et mécaniques couplées : Une approche thermo-élasto-plastique endommageable. *Thèse de doctorat de l'INSA de Lyon*: 207

Ulm, F.J. & Acker, P. 1998. Le Point sur le Fluage et la Recouvrance des Bétons. *Bulletin des Laboratoires des Ponts et Chaussées spécial XX:* 73-82. (*in french*)

[1] Electricité de France